Supporting Information for manuscript

# Viruses at solid-water interfaces:

# A systematic assessment of interactions driving adsorption

Antonius Armanious[1,2], Meret Aeppli[1], Ronald Jacak[3], Dominik Refardt[4],

Thérèse Sigstam[2], Tamar Kohn[2], Michael Sander[1,*]


1: Institute of Biogeochemistry and Pollutant Dynamics (IBP)

Department of Environmental Systems Science, ETH Zurich, Switzerland

2: Laboratory of Environmental Chemistry, School of Architecture, Civil and Environmental

Engineering (ENAC), École Polytechnique Fédérale de Lausanne (EPFL), Lausanne,

Switzerland

3: Johns Hopkins University Applied Physics Laboratory, Howard County,

Maryland 20723, United States

4: Institute of Integrative Biology (IBZ), Department of Environmental Systems Science,

ETH Zurich, Switzerland

Submitted as manuscript to *Environmental Science & Technology*

* Corresponding author:
Michael Sander
email: michael.sander@env.ethz.ch
Phone: +41 (0)44 632-8314; Fax: +41 (0)44 633-1122

Number of Figures:          19

Number of Tables:           1

Number of Pages:            39

**S1 Materials and Methods**

*S1.1 Modeling of the physicochemical properties of the virus capsids*

*S1.1.1 Crystallographic structures of the viruses*

The following RCSB PDB files were used for generating structures of the phage capsids: 2MS2[1] for MS2, 1FRS[2] for fr, 1GAV[3] for GA, and 1QBE[4] for Qβ. Chains A and C of the Qβ crystal structure are missing density for two loops (i.e., amino acid residues 56-60 and 76-79). We assumed that the missing conformations of these loops in chains A and C can be approximated by the known conformations of these loops in chain B. Thus, the coordinates for these missing loops in chains A and C were built using the chain B conformations. The coordinates of chain B were aligned to chains A and C using PyMOL,[5] and the superimposed coordinates for residues 52-62 and 73-83 were used in place of the corresponding residues in chains A and C. The validity of this modification to the structure file is supported by the small C-alpha RMSD of 0.30 $\text{Å}^2$ between residues 52-62 of chain A for the "grafted" structure and another Qβ capsid protein structure (PDB: 4L8H)[6] having density for this loop.

The VIPERdb[7] website was used to generate the whole capsid, half capsid and 12-trimer structures of the capsids for each of the viruses. The VIPERdb utility "PDB to VIPER" was used to create .vdb files from each of the downloaded PDB files and for the "grafted" 1QBE PDB file. The resulting 2MS2.vdb, 1FRS.vdb and 1GVA.vdb were used as generated. The resulting 1QBE-grafted.vdb file was aligned to the .vdb file that is generated for the unmodified 1QBE.pdb file. This alignment was required to ensure that there is no difference in the assignment of chains to oligomer subunits

compared to the other three capsid files (i.e., 2MS2.vdb, fr.vdb, and GA.vdb). The aligned 1QBE-grafted.vdb file was used as input to the VIPERdb "Oligomer Generator" function (using T=3 symmetry) to generate full and half capsid structures. The first 12 (chain A, B, and C) trimers in the half capsid file were used for the 12-trimer file. Most of the analyses were conducted using the 12-trimer structures, as detailed below.

*S1.1.2. Identifying the positions of amino acid residues in the capsids*

The amino acids in the capsids of the viruses were categorized as either lying on the outer capsid surface, on the inner capsid surface, or as buried in the capsid. The residues on the outer surfaces of the capsids (i.e., the residues facing away from the capsid towards the bulk solution) were identified by inspecting the 12-trimers files in the visualization software UCSF Chimera (Version 1.8.1; Chimera is developed by the Resource for Biocomputing, Visualization, and Informatics at the University of California, San Francisco, supported by NIGMS P41-GM103311)[8]. Amino acids were identified as buried if their solvent accessible surface area (SASA) values were less than 20% of their total SASA values (i.e., that are obtained for the amino acids in their totally solvent accessible form). SASA values were calculated per residue using the GetArea script (accessed 15th of July 2014) with a probe molecule radius of 1.4 Å.[9] The amino acids on the outer surface of the virus capsids are depicted in red in **Figure S1** (and listed in the attached excel file), while all other amino acids are shown in blue.
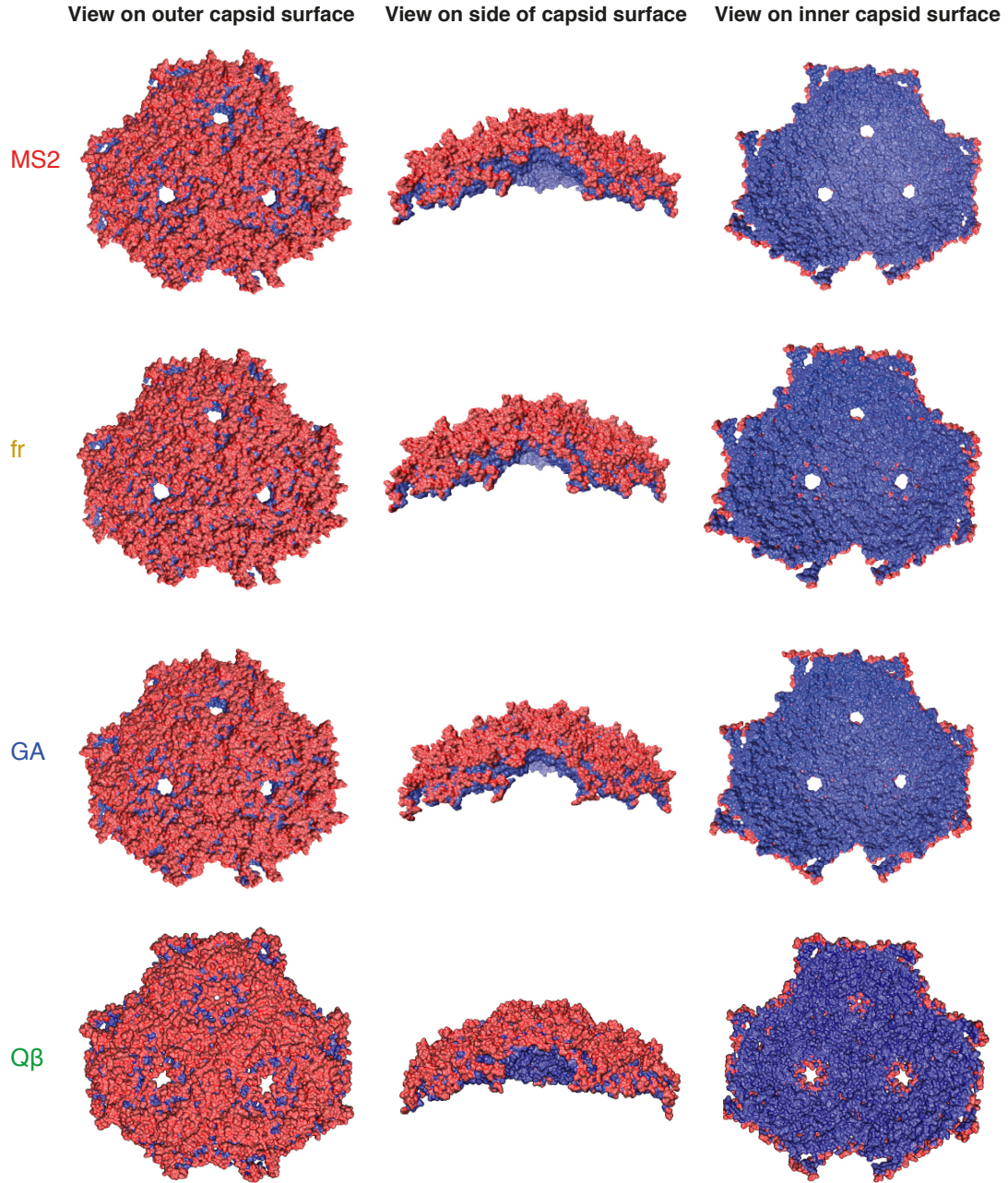
| View on outer capsid surface | View on side of capsid surface | View on inner capsid surface |
| --- | --- | --- |

MS2

fr

GA

Qβ



**Figure S1.** Depiction of the amino acids located on the outer surfaces of the capsids (shown in red) for bacteriophages MS2, fr, GA and Qβ. All remaining amino acids, located either on the inner surface of the capsids or buried in the capsids, are depicted in blue.

*S1.1.3 Charges of virus capsids*

Virus charge characteristics were computed from the amino acid (AA) compositions according to[10]:

$$\sigma = [\sum_i R_i H^+ - \sum_i R_i O^-] \frac{FN}{A} \qquad \text{Eq. S1}$$

where $\sigma$ (C·m$^{-2}$) is the charge density on the capsid surface, $R_iH^+$ and $R_iO^-$ are the total numbers of positive and negative charges per capsid protein trimer calculated based on estimated p$K_a$ values for each ionizable AA and the Henderson–Hasselbalch equation, $N$ (= 60 for all viruses) is the number of trimers per viral particle, $A$ (m$^2$) is the outer capsid surface area of virus assuming smooth spherical capsid of known diameter, and $F$ (=96485·10$^4$ C·mol$^{-1}$) is the Faraday constant. As mentioned in the manuscript, we performed two calculations. The first included all ionizable AAs in the capsids, and the second included only ionizable AAs located on the outer capsid surfaces facing the bulk solution.

We used the PROPKA protein model[11] to estimate the p$K_a$ values of the terminal amine groups, the terminal carboxyl groups and the ionizable amino acid residues (i.e., Arginine, Lysine, Aspartic Acid, Glutamic Acid and Tyrosine) in the capsid proteins. The calculations were carried out with the resolved crystallographic structure capsid protein trimers. Prior to the calculations, the PDB files were edited to contain only the atoms of the capsid proteins (i.e., all heteroatoms, such as atoms from water molecules, were removed from the files). The PROPKA model was applied using the PDB2PQR[12,13] software (version 1.9) on the webpage http://nbcr-222.ucsd.edu/pdb2pqr_1.9.0/ (accessed February, 2015). The p$K_a$ values of all the amino acid residues are listed in the attached excel file.

*S1.1.4 Polarity characteristics of the virus capsids*

*Hydropathy index plots.* The hydropath index plots calculations were run on http://web.expasy.org/protscale/ with a window of 5 AAs; accessed May 2015 as detailed in the manuscript.

*Hydrophobic patch scoring.* The polarity characteristics of the viruses were assessed using the protein design software *Rosetta*[14,15] and by applying a hydrophobic patch scoring system that increases exponentially with the total area of an individual apolar patch.[16]

Rosetta input structures were created and manipulated using custom Perl scripts. Lines beginning with tokens other than "ATOM" were stripped from the PDB files, and "TER" token lines were added after the end of every chain. Values ranging from 01 to 12, 30, or 60 were added to the 'segment id' field, characters 73-76 in ATOM coordinate lines as defined by the RCSB PDB file standard, of the 12-trimer, half capsid and whole capsid structures, respectively. Because of the one character limit to the chain id field in the PDB file format, only 62 unique chains are possible (A-Z, a-z, and 0-9). Addition of a segment id to the ATOM lines simplifies viewing and manipulating structures with more than 62 chains in PyMOL. The PyMOL selection logic reads segment id, in addition to chain id, residue number and insertion code, making it possible to address and select individual chains, even in 180 chain whole capsid structures. Finally, for any files used as input to Rosetta, the chain ids were also reset in the order A-Z, 0-9, a-z using a custom Perl script.

Calculations of hydrophobic patches were performed on structures containing all of the chains of the 12-trimer file plus surrounding chains (**Figure S2**). To generate these structures, the 12-trimer and whole capsid structures were loaded in PyMOL and superimposed. Chains neighboring the chains of the 12-trimer were determined through visual inspection and their segment id/chain id values were saved. The chains that were found to be neighboring the 12-trimer chains were as

follows (//segment-id/chain-id): //13/A, //13/C, //15/A, //16/A, //16/C, //17/C, //18/A, //18/B, //22/B, //23/A, //23/B, //23/C, //25/C, //26/A, //26/B, //26/C, //27/A, //27/B, //27/C, //28/B, //28/C, //29/A, //41/B, //59/A, //59/B, //60/C. Each of the 12-trimer plus neighbors structures ("expanded structures") for the various capsids were obtained by selecting segment ids 01-12 and the chains listed above from the whole capsid structures. The structures were then saved as pdb files. These expanded structures, instead of just the 12-trimer structures, were constructed and used to exclude hydrophobic patches from the analysis that start on the outer surface of the capsid but extend across the "edge" of the 12-trimer into the buried part and/or the inner surface of the capsid. The use of the extended structure therefore eliminated potential artifacts that arise from having edges in the 12-trimer structures (i.e., these edges do not exist in the complete capsid structures). We did not use whole capsid structures to calculate hydrophobic patch data, because the Rosetta modeling suite currently discards the segment identifier from input PDB files, making it difficult, though not impossible, to work with structures containing more than 62 chains.

Hydrophobic patch data for patches on the outer surface of the 12-trimer subunits were determined by first calculating the hydrophobic patch data over the 12-trimer plus neighboring chain structures (i.e., using the "extended structures"), and subsequently filtering out all hydrophobic patches that were buried and/or positioned on the inner surfaces of the substructures. In addition, we filtered out the hydrophobic patches that had most of their areas located on the chains neighboring the central 12-trimer structure. First, the Rosetta 'score' application was used to find all hydrophobic patches on each capsid 12-trimer structure and the neighboring chains structure

(Rosetta command line: *~/rosettabin/score.macosgccrelease -database ~/rosettadb/ -s [capsid]_12TrimerPlusNeighbors.rechained.pdb -resfile resfile.natro -score:weights talaris2013_hpatch.wts > log.[capsid]_12TrimerPlusNeighbors.rechained*). The log file generated from the Rosetta score application and the information on which residues are positioned on the outer capsid surfaces (as obtained from the SASA values and inspection in Chimera, see above) were supplied as parameters to a custom Perl script together with the 12-trimer plus neighbors structure file (extended 12-trimer structure). This Perl script iterates through all of the identified hydrophobic patches, and removes those that exist wholly on the inner surface of the capsid, that are buried, and that are positioned on the chains neighboring the 12-trimer structures. For patches spanning both the 12-trimer structure area and the neighboring chains, we discarded the patches for which more than half the atoms of the patches lied outside of the 12-trimer structures (i.e., patches for which more than half of the constituting atoms were positioned on the chains neighboring the central 12-trimer structures). Upon completion of the filtering, the Perl script outputs the total score of all hydrophobic patches on the 12-trimer structures and the corresponding PyMOL selection expressions for viewing the patches on these structures (**Figure S2**). By the virtue of symmetry of the capsid, the total score of the hydrophobic patches of the whole capsid were determined by multiplying the total score of the 12-trimer by five (i.e., 5 * 12 = 60 trimers).
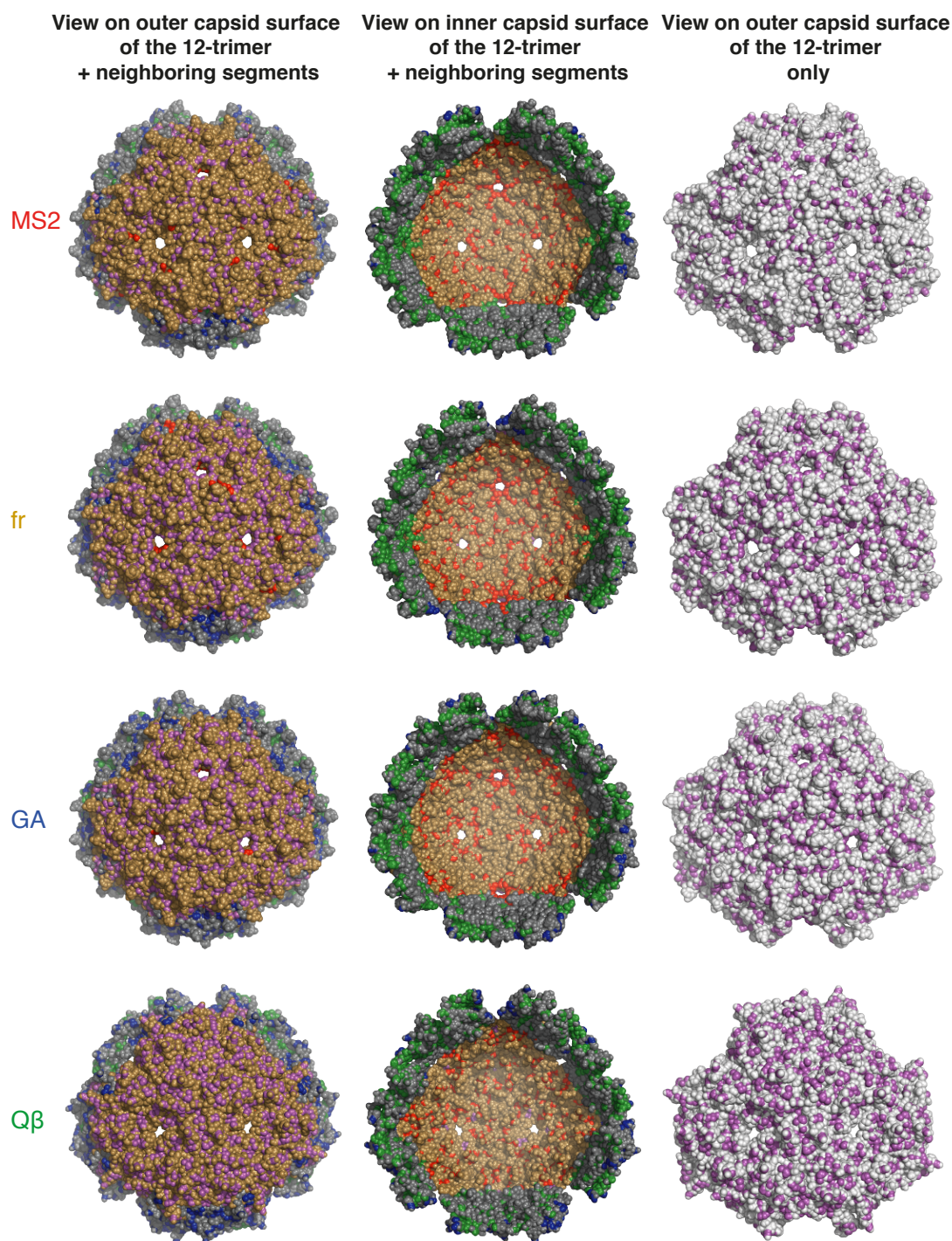
**View on outer capsid surface of the 12-trimer + neighboring segments**

**View on inner capsid surface of the 12-trimer + neighboring segments**

**View on outer capsid surface of the 12-trimer only**

MS2

fr

GA

Qβ

**Figure S2.** Depiction of hydrophobic patches on the 12-trimer structures and the neighboring chains of the four bacteriophages (i.e., MS2, fr, GA and Qβ). The following color coding was used: *gold* for the 12-trimer structure; *grey* for the neighboring chains; *magenta* for "true" hydrophobic patches located on the outer surface of the capsid and primarily on the 12-trimer; *red* for hydrophobic patches on the inner surface of the capsid and/or buried in the capsid but mostly on the 12-trimer (a small number of red patches that appear to be on the surface are in fact mostly buried); *blue* for hydrophobic patches which are mostly on the neighboring chains (minimal occupancy on the 12-trimer); and *green* for hydrophobic patches which are on the neighboring chains and also hitting residues on the inner surface and/or buried in the capsid.

*S1.2 Chemicals and dissolved organic matter (DOM) samples*

Cysteamine and Bis(2-hydroxyethyl)amino-tris(hydroxymethyl)methane (BIS-TRIS) were obtained from Sigma, tris(hydroxymethyl)aminomethane (TRIS), 11-Mercaptoundecanoic acid and 1-Dodecanethiol from Aldrich, anhydrous ethanol, ethanol, acetic acid, and sodium hydroxide from Fluka, and sodium chloride and hydrochloric acid from Merck. All chemicals were of analytical grade and used as received. The DOM samples included Standard Suwannee River humic and fulvic acid (i.e., SRHA and SRFA) and Elliot Soil humic acid (ESHA) that were obtained from the International Humic Substances Society (IHSS) and used as received.

*S1.3 Experimental solutions*

All solutions were prepared in MilliQ water (resistivity $\approx$ 18.2 M$\Omega$·cm; Barnstead NANOpure Diamond), and pH buffered using acetic acid (pH 5), bis(2-hydroxyethyl)amino-tris(hydroxymethyl)-methane (BIS-TRIS) (pH 6 and 7) and tris(hydroxyl-methyl)aminomethane (TRIS) (pH 8 and 9). The solution pH and total ionic strength, *I*, were adjusted with NaOH/HCl (each 1 M) and with sodium chloride, respectively.

*DOM solutions*. DOM stock solutions were prepared as detailed in Armanious et al. (2014).[17] In brief, 500 $\mu g_{DOM} \cdot mL^{-1}$ solutions were prepared by dissolving the respective HA or FA in MilliQ water. Following dissolution, the solutions were adjusted to pH 7, sterile filtered, divided in aliquots and stored at 4°C until use. To form DOM adlayers, defined volumes of the DOM aliquots were ten-fold diluted in

pH and $I$ pre-adjusted buffer solutions to obtain experimental DOM solutions with concentrations of 50 $\mu g_{DOM} \cdot mL^{-1}$ at the desired solution pH and $I$.

*Virus like particles (VLPs)*. VLPs of MS2 (MS2-VLP) were prepared according to Hooker et al (2004)[18] and as detailed in Wigginton et al (2012)[19]. In brief, the preparation procedure relies on the base-catalyzed hydrolysis of the ssRNA inside the MS2 capsid at high solution pH, followed by loss of the hydrolyzed ssRNA from the capsid. In a first step, solutions containing purified viruses were prepared by membrane filtration through 100 kDa Amicon Ultra-15 centrifugal filters, as detailed in the manuscript. Following the purification, the buffer of the purified virus solution was exchanged to a pH 11.8 buffer (i.e., 100 mM NaCl and 100 mM $Na_2HPO_4$) by two membrane filtration cycles (100 kDa Amicon Ultra-2 centrifugal filters). After the two cycles, the virus-containing retentate was re-suspended in 1–2 mL of pH 11.8 buffer and stored for 3–4 hours at room temperature. The solution was subsequently concentrated and washed once again using pH 11.8 buffer through 100 kDa Amicon Ultra-2 centrifugal filters. The prepared VLPs were washed for 3–4 cycles with buffer (5 mM $HPO_4^{2-}$, 10 mM NaCl, pH 7.4) through 100 kDa Amicon Ultra-2 centrifugal filters. Afterwards, the VLPs were washed again for at least 10 cycles through 100 kDa Amicon Ultra-15 centrifugal filters using the membrane filtration approach. We attempted —but were unsuccessful— to prepare VLPs also for GA and Qβ, indicating that the capsids of these two viruses were instable at pH 11.8.

*S1.4 Infectivity values and RNA and protein contents of the viruses and MS2-VLP*

The infectivity values of the virus solutions were determined by counting their plaque forming units (PFU) using the double agar layer method.[20] RNA contents of

the viruses were determined using a Nanodrop 1000 spectrophotometer (Thermo Scientific, Wilmington, DE, USA) by measuring absorbance of 1.5–2 µL samples at 260 nm and calculating the RNA concentrations based on Beer's law using the instrumental software Nanodrop ND-1000 (V.3.5.2(A)). The RNA contents of the MS2-VLP were determined with a Qubit™ RNA BR assay kit on a Qubit® 2.0 Fluorometer instrument (Thermo Fisher Scientific). This method accurately quantifies RNA contents over the range of 20–1000 ng RNA. This approach was taken because the RNA contents of the MS2-VLP were too small to allow for an accurate estimation using the Nanodrop absorbance measurement approach. The protein contents of the viruses and MS2-VLP were determined using a Qubit® 2.0 Fluorometer and a Qubit™ protein assay kit (with a quantification range between 0.25 and 5 µg protein). The results of these analyses are provided in **Table S1**.

*S1.5 Hydrodynamic diameters and electrophoretic mobilities of the viruses and MS2-VLP*

The hydrodynamic diameters and the electrophoretic mobilities of the viruses and MS2-VLP were determined using a Zetasizer Nano ZS instrument (Malvern Instruments, Malvern, UK). To assess the pH dependence of these parameters, the pH of the solutions were varied using an autotitrator (model MPT-2; Malvern, UK). The measurements were conducted using folded capillary cells (DTS1070). Prior to the measurements, all solutions used in the measurements (i.e., 0.1 M HCl and 0.1 M NaOH for pH titrations and 10 mM NaCl solutions prepared in MilliQ water) were filtered through 100 kDa filters. The measurements were conducted at a constant temperature of 20 ˚C. The solution pH values were systematically altered, starting at pH 9 and decreasing to pH 2 with steps of $\Delta pH = 1$. Zeta potentials, isoelectric points

(IEP) and sizes were evaluated using the Zetasizer software version 7.03 (Malvern, UK). The reported diameters were determined based on the measured number distributions of the particles. For most measurements, the reported diameters corresponded to 100% of the number distributions (i.e., the reported size was the only size detected). For a very few measurements, the reported diameters corresponded to less than 100% but always more than 98% of the measured number distributions. The concentrations of the viruses and MS2-VLP used in the measurements are provided in **Table S1**.

*S1.6 Sensor cleaning and purification for QCM-D adsorption experiments.*

Two types of QCM-D sensors were used: silica-coated sensors ($SiO_2$ sensors; QSX 301, QSense) and gold-coated sensors (Au sensors; QSX 301, QSense). The silica-coated sensors were cleaned by sonicating them for 15 minutes in a solution of sodium dodecyl sulfate (2% by weight), rinsing thoroughly with MilliQ water, and finally placing them in a UV/Ozone chamber for at least 30–40 min (Bioforce Nanoscience). The gold-coated sensors were additionally treated for 2 minutes with few drops of Piranha solution (3:1, concentrated $H_2SO_4$:$H_2O_2$ 30%; *piranha is a very aggressive oxidant and should be handled with uttermost care*), and then washed thoroughly with MilliQ water and subsequently with ethanol. The sensors were used directly after cleaning for the adsorption experiments.

*S1.7 Formation of self-assembled monolayers (SAMs) on gold-coated QCM-D sensors.*

A detailed protocol on the formation of SAMs is provided in Armanious et al. (2014).[16] First, gold-coated QCM-D sensors (QSX 301, QSense) were thoroughly

cleaned as detailed in the previous section. The cleaned sensors were then transferred to polypropylene reaction tubes containing alkylthiol solutions (0.5–2.0 mM) in anhydrous ethanol and left to react for at least twelve hours. The reaction was conducted in an anoxic glovebox with $N_2$ atmosphere to rule out oxidation of the thiol compounds by $O_2$. SAMs were formed from cysteamine (SAM-$NH_3^+$), 11-Mercaptoundecanoic acid (SAM-$COO^-$), and 1-Dodecanethiol (SAM-$CH_3$). Following formation of the SAMs, the sensors were rinsed and sonicated in ethanol to remove unbound alkylthiols and then directly used for adsorption experiments. Proper formation of SAMs was previously verified by ellipsometry and by contact angle measurements.[16]

*S1.8 Adsorption experiments*

A typical virus adsorption experiment to the model surfaces (i.e., SAM surfaces, Au, and $SiO_2$) consisted of three consecutive steps: (i) Sensor equilibration to obtain stable frequency and dissipation readings by continuously running adsorbate-free pH-buffered solutions over the surfaces of sensors mounted in the QCM-D flow cells. (ii) Assessment of virus adsorption to the surfaces by continuous delivery of virus-containing solutions through the flow cells. (iii) Rinsing with virus-free solutions. All three steps were conducted at a constant temperature (20 ˚C), constant volumetric flow rate (20 µL·$min^{-1}$), and a constant solution pH and ionic strength *I*.

Adsorption experiments to DOM adlayers were conducted using SAM-$NH_3^+$ surface-tailored sensors and consisted of two additional steps. Following step (i), DOM adlayers were formed on the SAM-$NH_3^+$ surfaces by continuous delivery of

DOM solutions (50 $\mu g_{DOM} \cdot mL^{-1}$) through the flow cells. The surfaces were subsequently rinsed with DOM-free solutions. Adsorption of viruses to the formed DOM adlayers was then assessed analogous to the adsorption to the model surfaces, as described above in steps (ii) and (iii). The concentrations of the viruses and MS2-VLP used in the adsorption experiments are provided in **Table S1**.

The fractional coverages of the sensor surfaces by viruses were estimated based on the hydration model of Bingen et al (2008),[21] assuming truncated pyramid hydration shells of the viruses (steepness of the sidewalls of the hydration shells, $k_s$ = 1.1), virus diameters of 28.8 nm, molecular weights of 3600 kDa, and virus densities of 1.42 g·cm$^{-3}$.[22] The Matlab script used for the calculations was downloaded from http://www.rrichter.net/ (accessed in March, 2015).

**S2 Results and Discussion**

*S2.1 Polarity of the virus capsid surfaces*

**Figure S3** shows the hydropathy index for the individual coat proteins of each of the four viruses. Positive and negative index values indicate hydrophobic (i.e., apolar) and hydrophilic (i.e., polar) amino acids (AAs), respectively. The colored sections correspond to AAs that were identified to lie on the outer surfaces of the capsids. While offering qualitative measures of the hydrophobicities of the coat proteins, the hydropathy index plots do not allow for direct and quantitative comparisons of the hydrophobicity of the viruses.
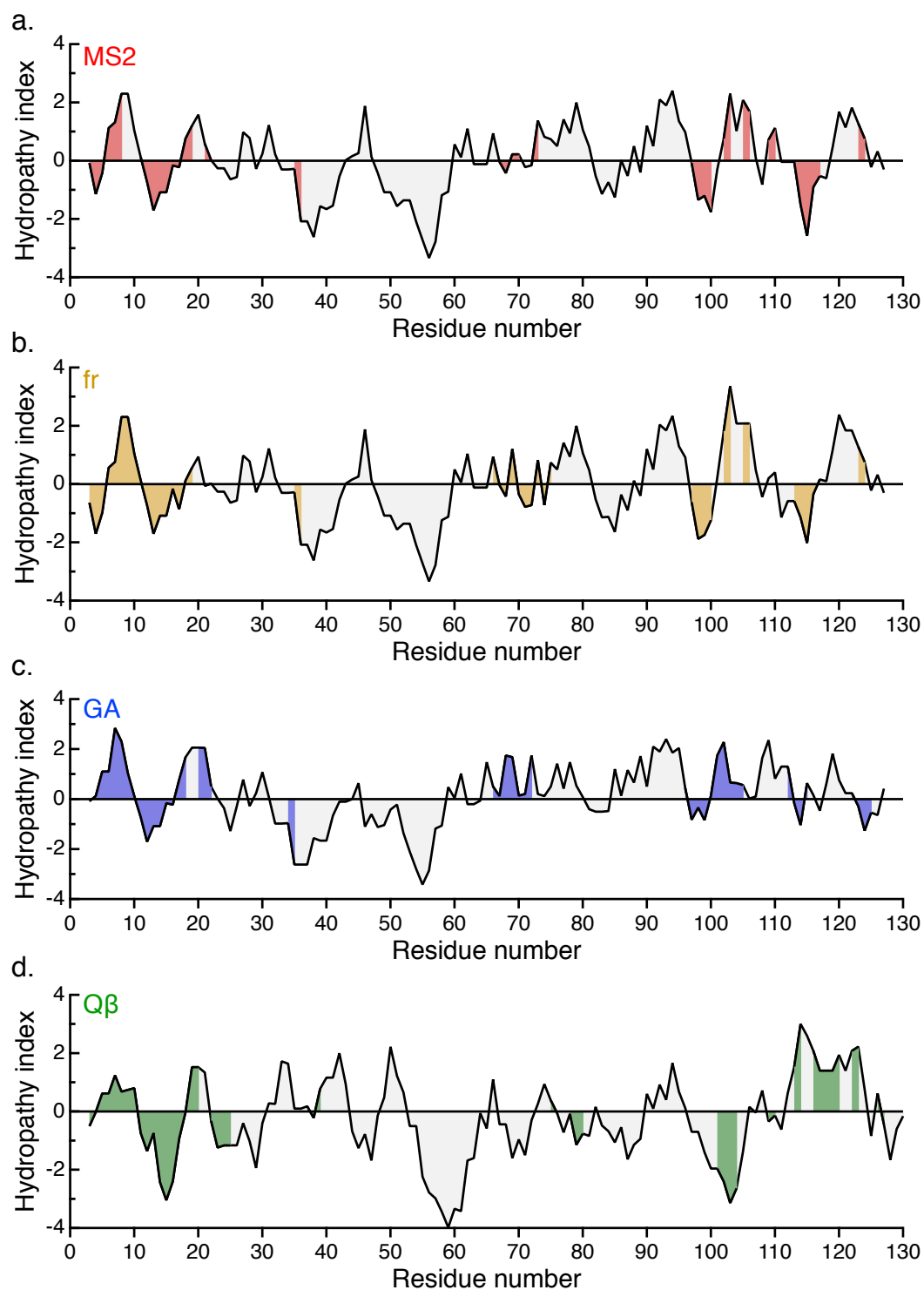
**Figure S3.** The hydropathy indexes for single capsid proteins of bacteriophages (a) MS2, (b) fr, (c) GA, and (d) Qβ. Positive values indicate hydrophobic amino acids and negative values hydrophilic amino acids based on the Kyte and Doolittle[23] scoring system. The colored sections indicate amino acids that are positioned on the outer surfaces of the virus capsids.

*S2.2 RNA and protein contents, infectivity values, and concentrations of viruses in experimental solutions*

**Table S1** provides the RNA and protein contents and the infectivity values of the experimental virus solutions. The RNA and protein contents suggest that most of the viruses contained full genomes in their capsids. The much lower RNA to protein contents of the MS2-VLP provides direct evidence for the removal of the ssRNA from the MS2 capsids. The low ratio of infective viruses to total viruses (i.e., ≲ 10%) is well established for bacteriophages.[24,25] The lower infectivity values of fr, GA and Qβ than of MS2 likely resulted from using the same host *Escherichia coli* strain (DSMZ 5695) which is known to be most susceptible to infections by MS2.

**Table S1**. RNA contents, protein contents, infectivity values, and concentrations of MS2, fr, GA, Qβ and MS2-VLP in experimental solutions.

| Virus | MS2 | fr | GA | Qβ | MS2-VLP |
|---|---|---|---|---|---|
| **RNA** | | | | | |
| MW (g·mol$^{-1}$)[a] | 1102321.8 | 1105773.6 | 1069846.1 | 1301995.3 | 1102321.8 |
| Mass (g per molecule) | $1.83 \cdot 10^{-18}$ | $1.84 \cdot 10^{-18}$ | $1.78 \cdot 10^{-18}$ | $2.16 \cdot 10^{-18}$ | $1.83 \cdot 10^{-18}$ |
| **Capsid** | | | | | |
| MW (g·mol$^{-1}$)[b] | 2515120.3 | 2539960.5 | 2507243.89 | 2614220.46 | 2515120.3 |
| Mass (g per molecule) | $4.18 \cdot 10^{-18}$ | $4.22 \cdot 10^{-18}$ | $4.16 \cdot 10^{-18}$ | $4.34 \cdot 10^{-18}$ | $4.18 \cdot 10^{-18}$ |
| **RNA content**[c] | | | | | |
| 260/280 absorbance | 1.87 | 1.85 | 1.79 | 1.94 | 0.77 |
| µg·mL$^{-1}$ | 42.9 | 86.4 | 139.7 | 51.6 | 0.27 |
| virions·mL$^{-1}$ | $2.3 \cdot 10^{13}$ | $4.7 \cdot 10^{13}$ | $7.9 \cdot 10^{13}$ | $2.4 \cdot 10^{13}$ | $1.5 \cdot 10^{11}$ |
| **Protein content**[d] | | | | | |
| µg·mL$^{-1}$ | 105.25 | 235.4 | 341.5 | 104.25 | 42.225 |
| virions·mL$^{-1}$ | $2.5 \cdot 10^{13}$ | $5.6 \cdot 10^{13}$ | $8.2 \cdot 10^{13}$ | $2.4 \cdot 10^{13}$ | $1.0 \cdot 10^{13}$ |
| **Infective, RNA-containing, and RNA-free capsids** | | | | | |
| Infectivity (PFU·mL$^{-1}$)[e] | $10^{12}$ | $4 \cdot 10^{11}$ | $6 \cdot 10^{11}$ | $2 \cdot 10^{11}$ | 0 |
| Ratio of RNA-containing capsids to the total number of capsids | 0.93 | 0.84 | 0.96 | 0.99 | 0.01 |
| Ratio of infective viruses to RNA-containing capsids | 0.04 | 0.01 | 0.01 | 0.01 | 0 |
| **Concentrations (virions·mL$^{-1}$)**[f] | | | | | |
| Adsorption experiments | $6.3 \cdot 10^{11}$ | $1.4 \cdot 10^{12}$ | $4.1 \cdot 10^{12}$ | $6.0 \cdot 10^{11}$ | $5.0 \cdot 10^{11}$ |
| Zeta potential and DLS measurements | $1.3 \cdot 10^{12}$ | $1.4 \cdot 10^{12}$ | $4.1 \cdot 10^{12}$ | $1.2 \cdot 10^{12}$ | $2.0 \cdot 10^{12}$ |

[a] The molecular weights of the ssRNAs of each virus were calculated using Oligo calc. (http://www.basic.northwestern.edu/biotools/oligocalc.html; accessed on January 2015). [b] Calculated for 180 copies of the capsid proteins and 1 copy of the A proteins. [c] RNA contents of the MS2, fr, GA and Qβ were determined by absorbance measurements using a NanoDrop 2000 instrument (Thermo, Washington, USA). The RNA content of the MS2-VLP was determined using a QuBit 2.0 fluorometer and a Q32855 Kit (Life Technologies, Thermo Fisher Scientific Brand). The RNA contents were quantified once for each virus in experimental virus solutions after the final purification step. It is possible that the RNA contents slightly varied between adsorption experiments due to variations in the virus recoveries in the final purification step. [d] Protein contents were determined using a Q33211 Kit and a QuBit 2.0 fluorometer (Life Technologies, Thermo Fisher Scientific Brand). The protein contents were quantified once for each virus in experimental virus solutions after the final purification step. It is possible that the protein contents slightly varied between adsorption experiments due to variations in the virus recoveries in the final purification step. [e] Infectivity values were determined using the double agar method with *Escherichia* coli (DSMZ 5695) as host. [f] Concentration values were calculated based on the protein contents.

**Figure S4** shows the absorbance spectra of solutions containing MS2 and MS2-VLP over the wavelength range of 220–360 nm. The ratio of absorbance intensities at 260 nm to 280 nm can be used to determine the RNA contents of the samples.[18] Removal of the RNA in the preparation of the MS2-VLP resulted in decrease in the absorbance ratio (260nm/280nm) from approximately 1.9 to 0.8. These results support the successful preparation of MS2-VLP.
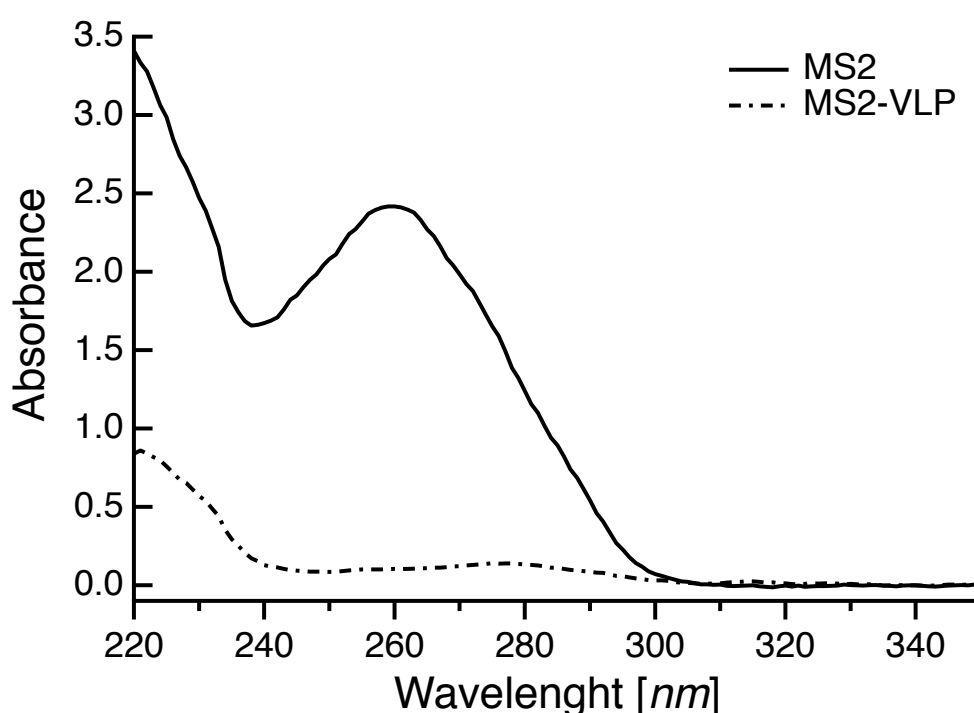


**Figure S4.** Absorbance spectra of solutions containing MS2 and MS2-VLP over the wavelength range 220–360 nm.

*S2.3 Adsorption of viruses to SAM-NH$_3^+$ surfaces*

**Figure S5** shows the changes in resonance frequencies, $\Delta f_n/n$, and dissipation energies, $\Delta D_n$ (panels on the left side) and the corresponding changes in adsorbed masses (panels on the right side) for the adsorption of fr, GA, Qβ, and MS2-VLP to SAM-NH$_3^+$ surfaces at pH 6 and $I$ = 10 mM (adjusted with NaCl). The adsorbed masses were calculated from the $\Delta f_n/n$ values using the Sauerbrey equation.
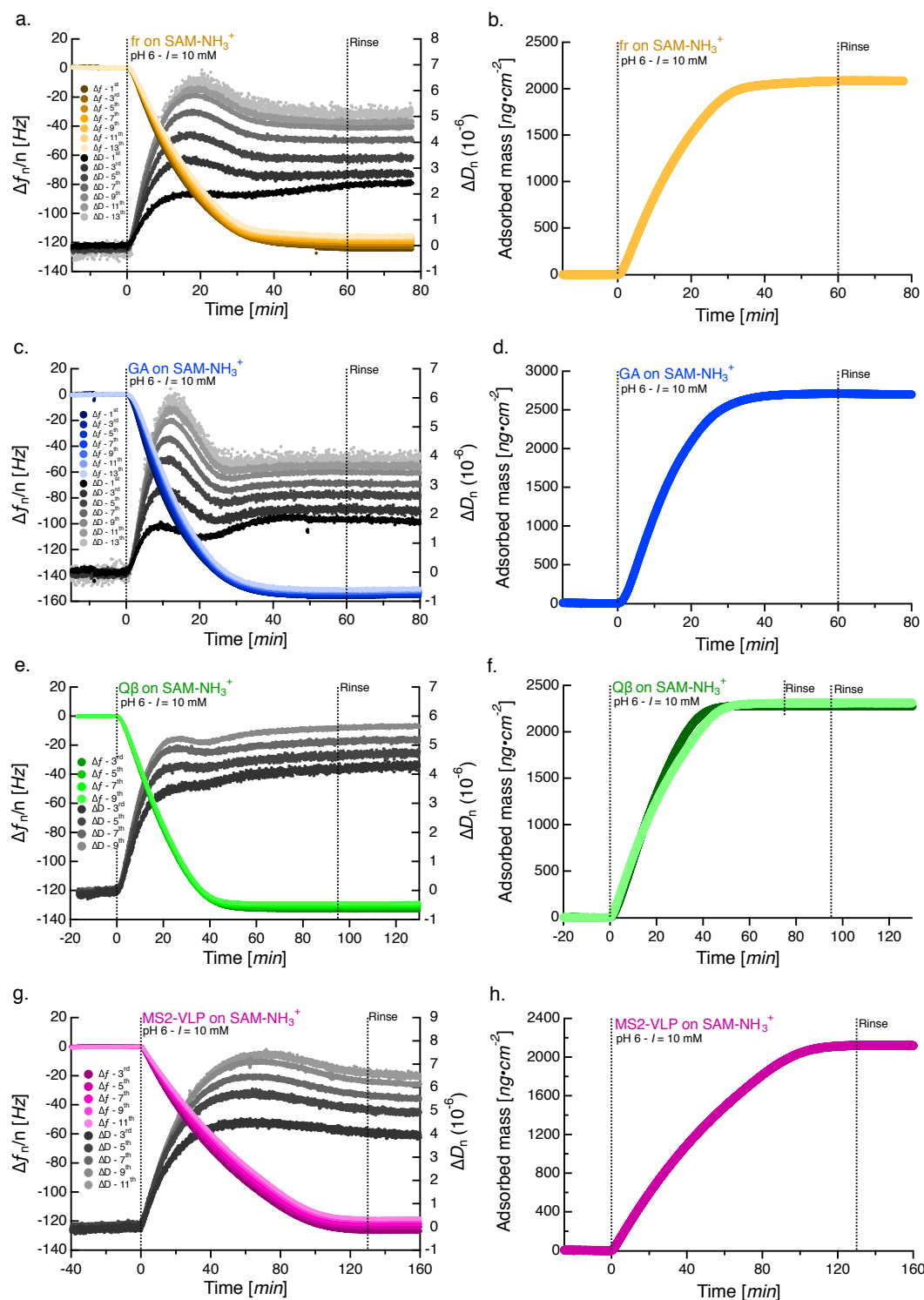
**Figure S5.** Adsorption profiles of bacteriophages fr, GA, Qβ, and MS2-VLP to amine-terminated self-assembled monolayer (SAM-NH$_3^+$) surfaces. Changes in the resonance frequencies ($\Delta f_n/n$) and in energy dissipation values ($\Delta D_n$) upon the adsorption of (a) fr, (c) GA, (e) Qβ, (g) MS2-VLP to SAM-NH$_3^+$ surfaces. The corresponding changes in adsorbed masses were calculated using the Sauerbrey equation and are shown in panels (b) for fr, (d) for GA, (f) for Qβ, and (h) for MS2-VLP. Panel f also shows the adsorption profile of a replicate Qβ experiment, demonstrating the high reproducibility of the QCM-D measurement approach. All experiments were conducted at pH 6 and $I$ = 10 mM with NaCl as a background electrolyte.

S20

**Figure S6** shows the initial adsorption rates of MS2, fr, GA, Qβ, and MS2-VLP on SAM-NH$_3^+$ surfaces versus the concentrations of the viruses and MS2-VLP in the experimental solutions. The concentrations of the viruses and MS2-VLP may have slightly varied from one adsorption experiment to another as a result of different virus recoveries during the final virus purification steps when preparing experimental solutions from the virus stock solutions. The linear increase in initial adsorption rate with increasing virus concentration supports that initial adsorption rates were diffusion-limited due to the absence of an energy barrier to adsorption (i.e., electrostatic attraction between the negatively charged viruses and MS-VLP and the positively charged SAM-NH$_3^+$ surfaces).
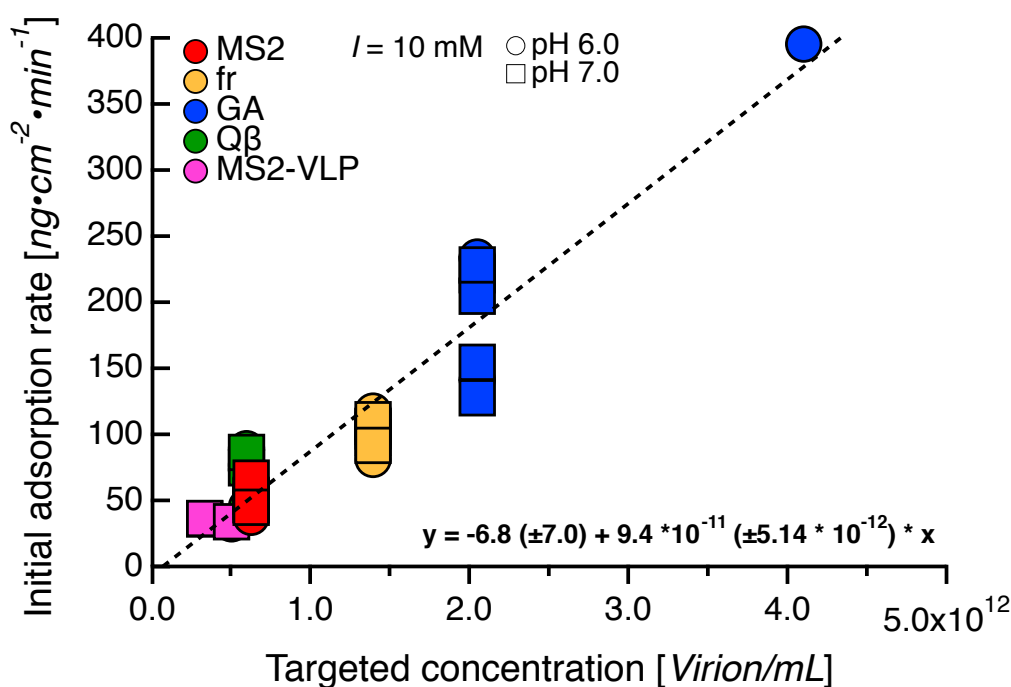


**Figure S6.** Initial adsorption rates of MS2, fr, GA, Qβ, and MS2-VLP to amine-terminated self-assembled monolayer (SAM-NH$_3^+$) surfaces as a function of the solution concentrations of the viruses and MS2-VLP at pH 6 and 7 and an ionic strength *I* of 10 mM, adjusted with NaCl. Uncertainties in the virus concentrations are not shown. These uncertainties are expected to be small and to originate from slightly different virus recoveries during final purification step when preparing experimental virus solutions from the respective virus stock solutions.

**Figure S7** shows the estimated change in surface coverage as a function of the adsorbed virus mass measured by QCM-D. The calculations were based on the hydration model developed by Bingen et al (2008).[21]
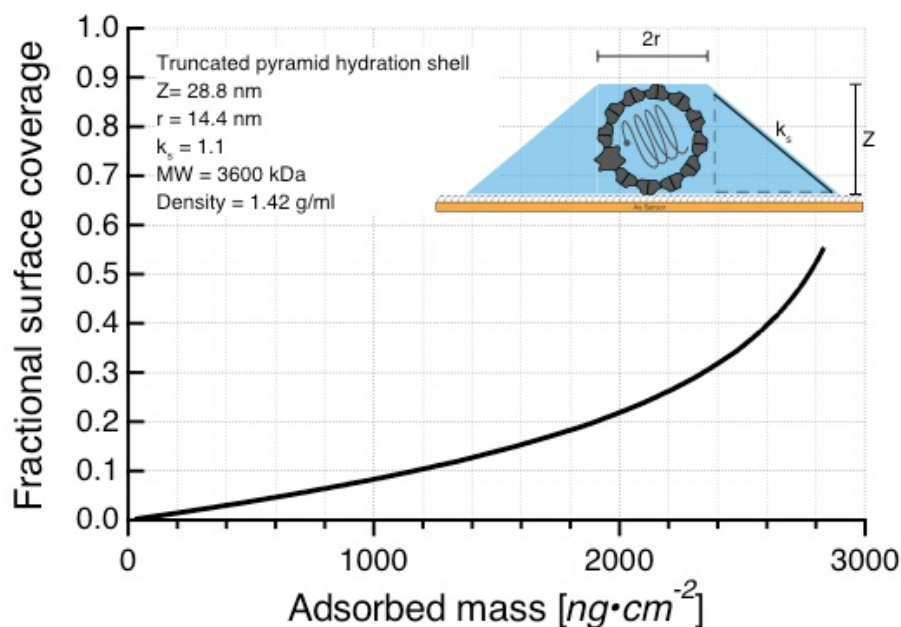


**Figure S7**. Estimated fractional surface coverages as a function of the adsorbed virus masses. The estimations are based on the hydration model developed by Bingen et al (2008).[21]

**Figure S8** shows selected adsorption profiles of MS2, fr, GA, Qβ, and MS2-VLP to SAM-NH$_3^+$ surfaces at pH 6 and $I$ = 10 mM (adjusted with NaCl) plotted as changes in the resonance frequency of the ninth overtone ($\Delta f_9/9$) versus changes in the energy dissipation values of the same overtone ($\Delta D_9$). The adsorption profiles of all viruses and the MS2-VLP exhibited pronounced maxima in the $\Delta D_9$ values at intermediate stages of adsorption (i.e., around $\Delta f_9/9$= -90 Hz). Similar maxima in the dissipation values were previously reported for the adsorption of spherical molecules to QCM-D sensor surfaces and were shown to results from the onset of hydrodynamic coupling between adjacent spherical particles on the adsorbent surfaces.[26] This hydrodynamic coupling leads to a reduction of the energy dissipation values because the lateral movement of the particles caused by the sensor oscillation becomes

restricted. This stabilization effect is observed only for surfaces that reach extensive coverages (i.e., beyond 10 to 20%). The adsorption of the four viruses continued beyond the maxima in dissipation values and thus reached even higher final surface coverages (i.e., that likely corresponded to the jamming limits under the given experimental conditions).
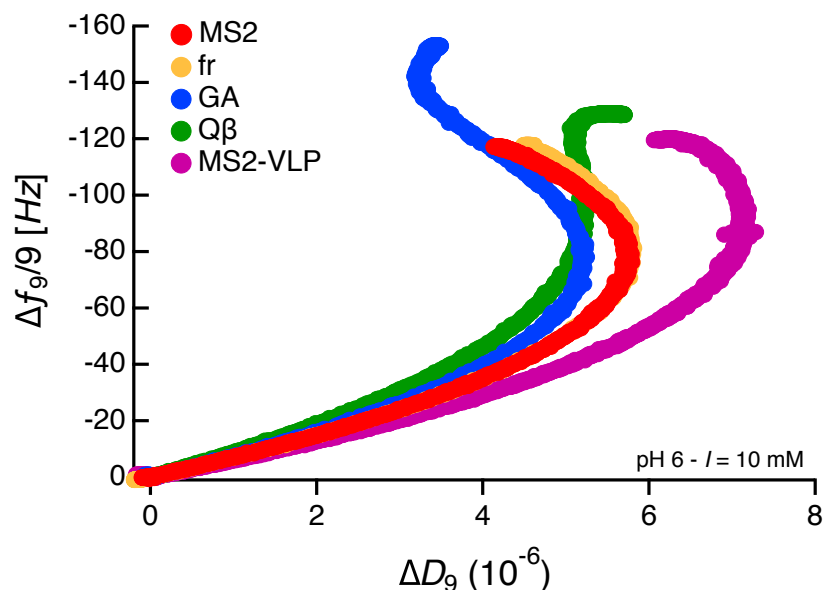


**Figure S8.** Adsorption profiles of MS2, fr, GA, Qβ, and MS2-VLP to amine-terminated self-assembled monolayers (SAM-NH$_3^+$) surfaces at pH 6 and $I$ = 10 mM (adjusted with NaCl) plotted as changes in the resonance frequency values ($\Delta f_9/9$) versus the changes in energy dissipation values ($\Delta D_9$) of the ninth oscillation overtone (n= 9).

*S2.4 Effects of virus purification protocols on virus adsorption profiles*

**Figure S9a** shows the adsorption profiles of MS2 obtained from different virus solutions to positively charged SAM-NH$_3^+$ surfaces and to positively charged poly-L-lysine (PLL) surfaces (obtained by immobilizing PLL on negatively charged SiO$_2$ sensors). We included PLL surfaces in these experiments because these surfaces have been used extensively in past studies to obtain positively charged surfaces for virus adsorption.[27,28] All experiments were conducted at pH 7 and $I$ = 50 mM with NaCl as a background electrolyte.

The tested MS2 solutions were obtained using different purification protocols. MS2 solutions purified by membrane centrifugation (i.e., no polyethylene glycol purification step; labeled "no PEG") resulted in very similar adsorption profiles on both the SAM-NH$_3^+$ and PLL surfaces. This finding suggests comparable jamming limits of MS2 on both surfaces. Adsorption profiles obtained from MS2 solutions prepared with a PEG step (labeled "PEG-washed" and "PEG-not washed") showed much lower final adsorbed masses as compared to the profiles obtained from MS2 solutions prepared without the use of PEG. The use of PEG in the purification protocol therefore suppressed MS2 adsorption and even caused MS2 desorption (see pronounced maxima in adsorbed masses for MS2 solution prepared with PEG and not washed). This suppression was evident even for the MS2 solution that was extensively washed with buffer solutions and purified using 100 kDa Amicon Ultra-15 centrifugal filters prior to the adsorption experiment (labeled "washed").

Based on these data, we recommend that PEG treatment steps should be omitted from virus purification protocols because the presence of PEG results in adsorption artifacts. A similar recommendation was recently made by Dika et al. (2013) who demonstrated that purification with PEG also affected the coagulation dynamics and electrophoretic mobilities of viruses in solution.[29]

**Figure S9b** shows two adsorption profiles of GA to SAM-NH$_3^+$ surfaces: both experiments were conducted at pH 6 and $I$ = 10 mM with NaCl as a background electrolyte. The adsorption profile with the higher final adsorbed mass (approximately 2600 ng·cm$^{-2}$) was obtained by using the purified GA solution in the QCM-D adsorption experiment immediately after the solution was prepared, as detailed in the

manuscript. The second adsorption profile with a lower final adsorbed mass (approximately 1900 ng·cm$^{-2}$) was obtained by using the same purified GA solution but this time five hours (and not immediately) after the solution preparation. The lower initial adsorption rate and lower final adsorbed GA mass obtained from the stored GA solution suggest that a significant fraction of the GA virus capsids had disintegrated during 5h storage at room temperature, possibly forming smaller capsid fragments, protein oligomers, and free ssRNA. Based on these findings, we suggest that virus adsorption experiments are run immediately after purified solutions are obtained.
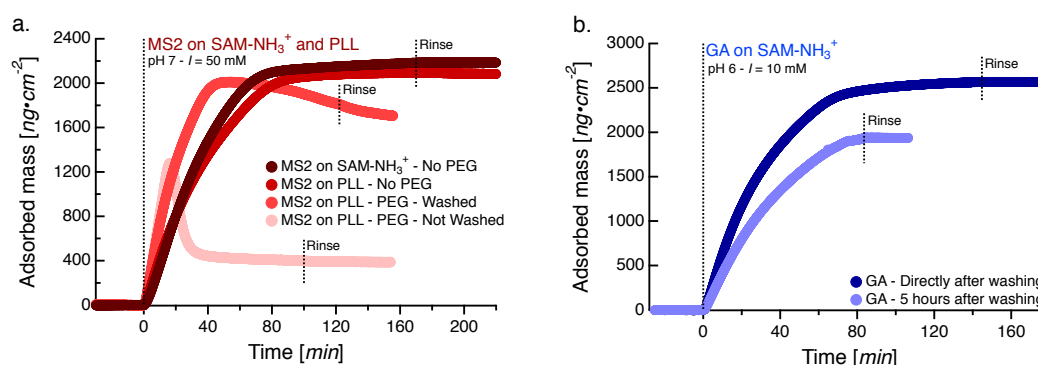


**Figure S9.** Assessment of effects of virus purification procedures and of time delay between virus purification and start of the adsorption experiment on virus adsorption profiles, as measured by quartz crystal microbalance with dissipation monitoring (QCM-D). (a) Adsorption profiles of MS2 to positively charged poly-L-lysine (PLL) surfaces and to amine-terminated self-assembled monolayers (SAM-NH$_3^+$). The MS2 solutions were prepared with different purification protocols. "No PEG": solutions obtained by membrane filtration omitting a polyethylene glycol (PEG) treatment step. "PEG − not washed": use of a PEG step in the purification, no membrane filtration. "PEG-Washed": use of a PEG step in the purification, washed using membrane filtration. All experiments were conducted at pH 7 and an ionic strength $I$= 50 mM with NaCl as the background electrolyte. (b) Adsorption profiles of GA to SAM-NH$_3^+$ surfaces using purified virus solutions directly after and five hours after the purification procedure was finished (i.e., labeled as "directly after washing" and "5 hours after washing", respectively). Both experiments were conducted at pH 6 and $I$ = 10 mM with NaCl as the background electrolyte.

*S2.5 Adsorption of MS2, fr, GA and Qβ to model surfaces*

  **Figures S10, S11, S12** and **S13** show representative adsorption profiles of MS2, fr, GA, and Qβ to SAM-COO$^-$, SiO$_2$, SAM-CH$_3$, and Au surfaces, respectively, measured at pH 5 to 8. All experiments were conducted at $I$= 10 mM with NaCl as the

background electrolyte. **Figure S14** shows representative adsorption profiles of MS2, and Qβ to SAM-NH$_3^+$, SAM-COO$^-$, SiO$_2$, SAM-CH$_3$, and Au surfaces, at pH 8 and $I$ = 10 to 100 mM with NaCl as background electrolyte.
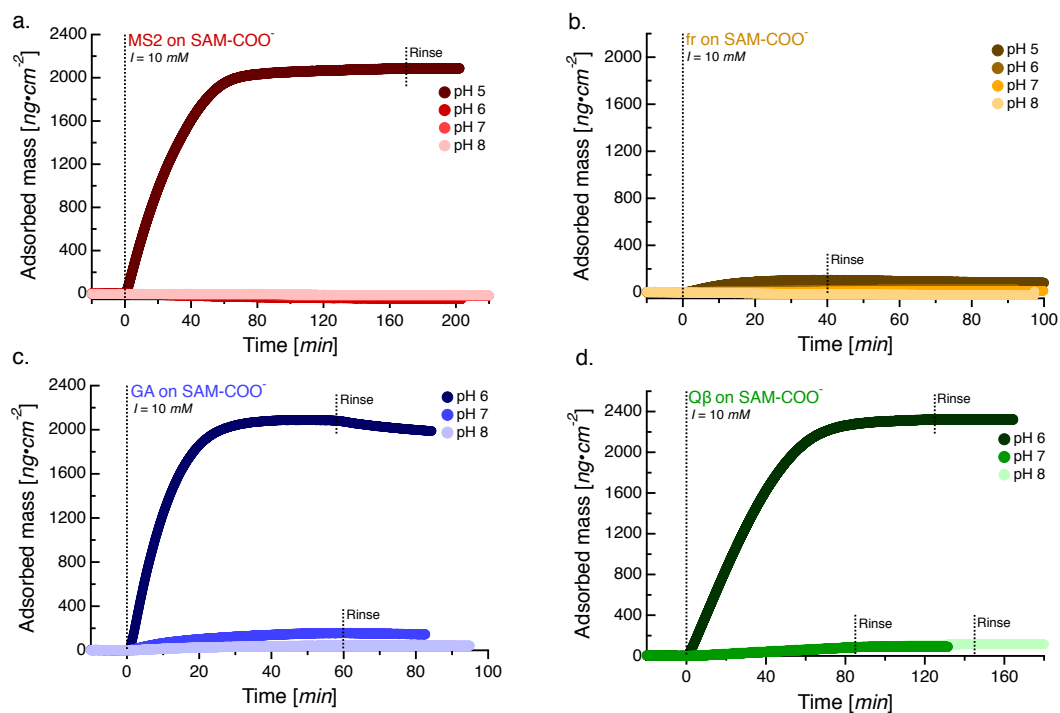


**Figure S10**. Adsorption profiles of (a) MS2, (b) fr, (c) GA, and (d) Qβ onto carboxyl terminated self-assembled monolayer (SAM-COO$^-$) surfaces at pH 5 to 8. All experiments were conducted at an ionic strength $I$ of 10 mM with NaCl as background electrolyte.
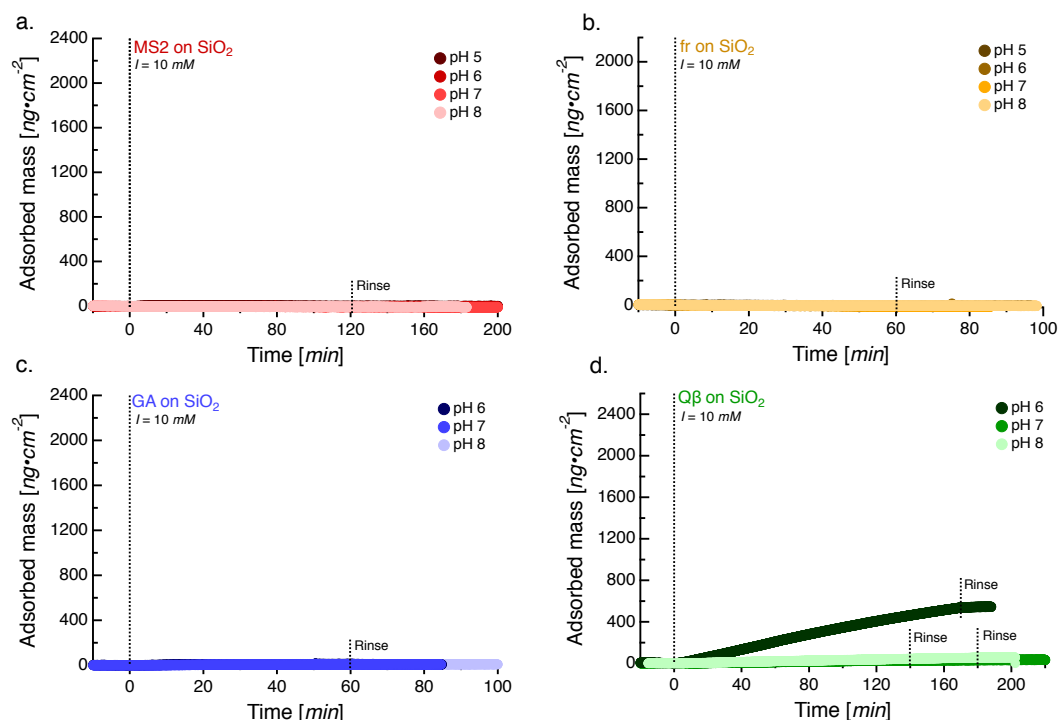
**Figure S11**. Adsorption profiles of (a) MS2, (b) fr, (c) GA, and (d) Qβ onto amorphous silica ($SiO_2$) surfaces at pH 5 to 8. All experiments were conducted at an ionic strength *I* of 10 mM with NaCl as background electrolyte.
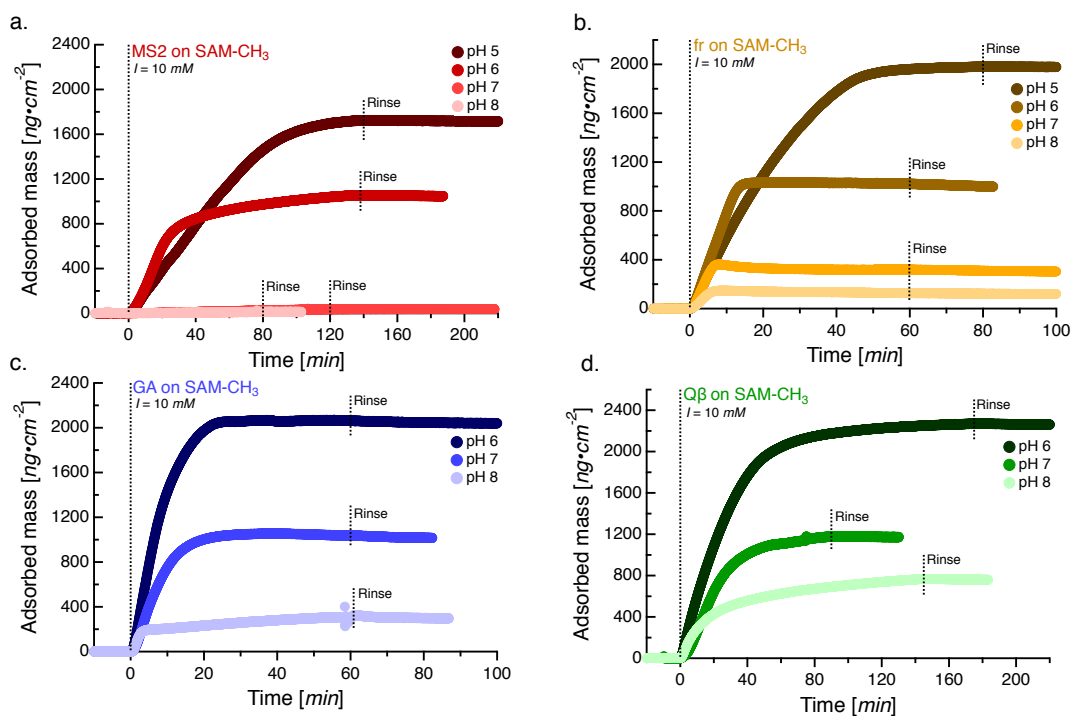


**Figure S12**. Adsorption profiles of (a) MS2, (b) fr, (c) GA, and (d) Qβ onto methyl terminated self-assembled monolayers (SAM-$CH_3$) surfaces at pH 5 to 8. All experiments were conducted at an ionic strength *I* of 10 mM with NaCl as background electrolyte.
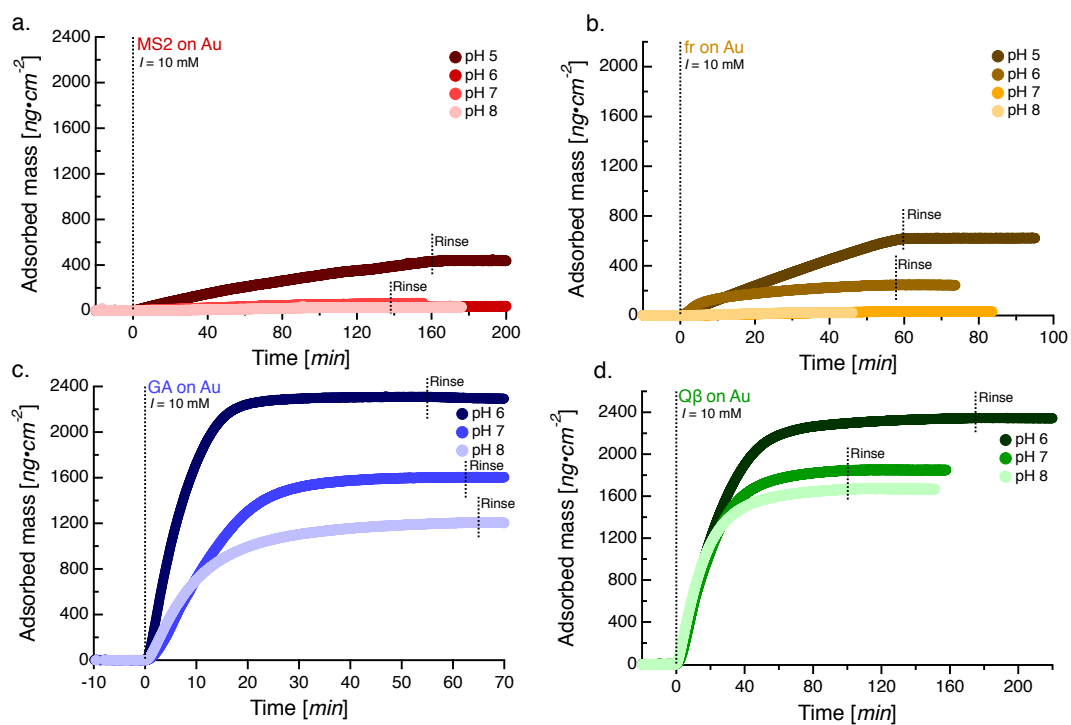
**Figure S13**. Adsorption profiles of (a) MS2, (b) fr, (c) GA, and (d) Qβ onto gold (Au) surfaces at pH 5 to 8. All experiments were conducted at an ionic strength $I$ of 10 mM with NaCl as background electrolyte.
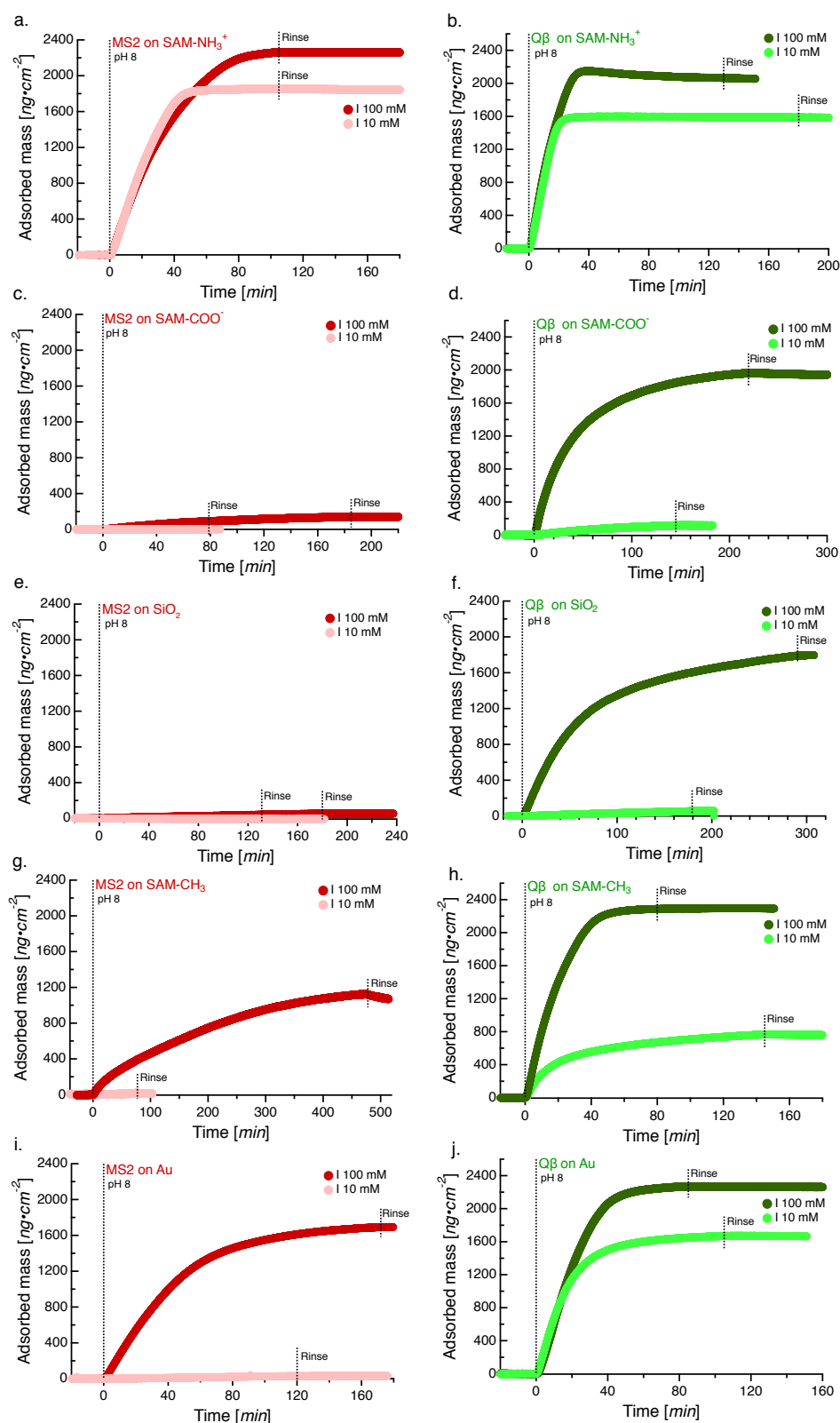
**Figure S14.** Adsorption profiles of MS2 (panels a, c, e, g, and i) and Qβ (panels b, d, f, h, and j) onto amine terminated self-assembled monolayer (SAM-NH$_3^+$) surfaces, carboxyl terminated SAMs (SAM-COO$^-$) surfaces, amorphous silica (SiO$_2$) surfaces, methyl terminated SAMs (SAM-CH$_3$) surfaces, and gold (Au) surfaces at pH 8 and at ionic strengths $I$ of 10 and 100 mM, adjusted with NaCl as background electrolyte.

*S2.6. DLVO theory*

**Figure S15** shows the calculated DLVO potential energy profiles of fr as a function of distance from planar SAM-CH$_3$ and Au surfaces, all at pH 8 and $I=10$ mM. The potential energy profiles were calculated using standard DLVO theory that accounts for both van der Waals interactions and electrostatic double layer interactions. The retarded van der Waals energy potential profile was calculated according to Gregory (1981)[30]:

$$W_{vdW} = -\frac{A_{132}R}{6D(1+^{14D}/_{\lambda})}$$

Eq. S2

where $W_{vdW}$ (J) is the potential due to van der Waals interactions, $A_{132}$ (J) is the Hamaker constant between particle 1 (virus) and surface 2 in medium 3 (water), $R$ (m) in the radius of the virus, $D$ (m) is the distance between the virus and the planar surface and $\lambda$ ($10^{-7}$ m) is the characteristic wavelength of interaction. For $A_{132}$ values we used estimated values reported by Murray and Parks (1980)[31] for the interactions of viruses with silica and metal surfaces: $A_{Virus-Water-SiO_2} \simeq A_{Virus-Water-SAMs} \simeq 0.4 \cdot 10^{-20} J$ (we consider this to be a conservative assumption because $A_{Virus-Water-SAMs}$ is expected to be lower than $A_{Virus-Water-SiO_2}$ due to the lower polarizability of the organic SAMs compared to silica)[32] and $A_{Virus-Water-Au} \simeq 3 \cdot 10^{-20} J$.

The electrostatic double layer interactions was calculated based on the equation from Hogg et al (1966)[33]:

$$W_{EDL} = (\pi R \varepsilon_0 \varepsilon_r)\{2\psi_1\psi_2 \ln\left(\frac{1+e^{-\kappa D}}{1-e^{-\kappa D}}\right) + (\psi_1^2 + \psi_2^2)\ln(1 - e^{-2\kappa D})\}$$

Eq. S3

where $W_{EDL}$ (J) is the potential due to electrostatic double layer interactions, $R$ (m) is the radius of the virus, $\varepsilon_0$ (= $8.854 \cdot 10^{-12}\ C^2 \cdot J^{-1} \cdot m^{-1}$) is the vacuum permittivity, $\varepsilon_r$ (= 78.4) is the relative permittivity for water, $\psi_1$ (= $-0.035\ V$ at pH 8 and $I$= 10 mM) is the surface potential of the virus, $\psi_2$ ($V$) is the surface potential of sorbent surface, $\kappa$ (= $3.3173 \cdot 10^8\ m^{-1}$ at $I$= 10 mM) is the inverse Debye length, and $D$ (m) is the distance between the virus and the surface. The surface potentials of sorbent surfaces were calculated using the Grahame equation[34]:

$$\sigma = \sqrt{8\varepsilon_0 \varepsilon_r k_B T}\ \sinh\left(\frac{e\psi}{2k_B T}\right) \sqrt{[NaCl]} \qquad\qquad \text{Eq. S4}$$

where $\sigma$ (C•m$^{-2}$) is the surface charge density, $\varepsilon_0$ (= $8.854 \cdot 10^{-12}\ C^2 \cdot J^{-1} \cdot m^{-1}$) is the vacuum permittivity, $\varepsilon_r$ (= 78.4) is the relative permittivity for water, $k_B$ (= $1.381 \cdot 10^{-23} J \cdot K^{-1}$) is the Boltzmann constant, T (K) is the temperature, $e$ (= $1.602 \cdot 10^{-19}\ C$) is the elementary charge, $\psi$ ($V$) is the surface potential, and $[NaCl]$ (m$^{-3}$) is the concentration of NaCl. For T = 293.15 K, $[NaCl]$ in M and $\psi$ in mV:

$$\sigma = 0.116\ \sinh\left(\frac{\psi}{50.5}\right) \sqrt{[NaCl]} \qquad\qquad \text{Eq. S5}$$

or

$$\psi = 50.5\ \text{arcsinh}\left(\frac{\sigma}{0.116\sqrt{[NaCl]}}\right) \qquad\qquad \text{Eq. S6}$$

The use of Eq. S6 resulted in $\psi_{SAM-CH_3} = -0.024\ V$ and $\psi_{Au} = -0.007\ V$ at

pH 8 and $I$= 10 mM based on the measured zeta potentials of SAM-CH$_3$ (at pH 8 and

$I$= 0.3 mM)[35] of ≈ -0.09 V and of Au (at pH 8 and $I$= 1 mM)[3] of ≈ -0.02 V [36].

Figure S15 a,b show the calculated potential profiles for vdW interactions and

electrostatic interactions as well as the summed potentials between fr and the SAM-

CH$_3$ and the Au surfaces, respectively. The summed potential profile in Figure S15a

shows an energy barrier of ≈ 10 k$_B$T at a separation distance of about D= 1 nm and no

secondary energy minimum at larger separation distances. Based on the pronounced

energy barrier, no adsorption of fr to the SAM-CH$_3$ surface would be expected. This

stands in contrast to the experimental data that showed pronounced adsorption of fr to

SAM-CH$_3$. We ascribe the discrepancy between modeled (no adsorption) and

experimental data (pronounced adsorption) to favorable contributions from the

hydrophobic effect to adsorption that are not captured by DLVO theory. Conversely,

the summed potential profiles in Figure S15b have negative values across the

modeled separation distance, suggesting that there is no energy barrier and hence that

fr should readily and extensively adsorb to the Au surface. Yet, the experimental data

showed only very little adsorption of fr to Au. This discrepancy between modeled

data (adsorption) and experimental data (no adsorption) may result from an

underestimation of the negative surface charge of Au (and hence electrostatic

repulsion) in the model and/or from steric hindrance to fr adsorption due to protein

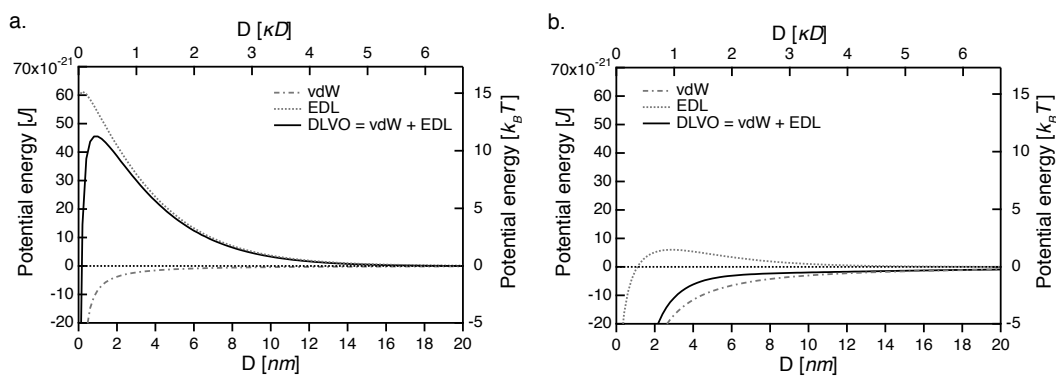loops extending from its capsid surface (see Figure 1 in manuscript).

**Figure S15.** Calculated DLVO potential energy profiles of fr as a function of separation distance D from the sorbent surface. The calculations were carried out for (a) methyl-terminated self-assembled monolayers (SAM-CH$_3$) and (b) Au surfaces, both for pH 8 and an ionic strength of $I$= 10 mM. The potential profiles were calculated using DLVO theory that accounts for both van der Waals interactions (vdW) and electrostatic double layer interactions (EDL).

*S2.7 Adsorption of MS2, fr, GA, Qβ, and MS2-VLP to DOM adlayers*

**Figure S16a** shows the results of representative adsorption experiments of MS2 and Qβ to SRHA adlayers at pH 6 and $I$ = 10 mM. The adsorption profiles also show the initial SRHA adsorption step: following equilibration of the SAM-NH$_3^+$ sensor to adsorbate-free solutions and the attainment of stable frequency readings, a SRHA-containing solution was delivered through the flow cells (start at approximately t= -50 min), resulting in the adsorption of SRHA to the SAM-NH$_3^+$ sensor surface. The formed SRHA adlayer was stable and did not desorb upon buffer rinsing (started at about t= -25 min), consistent with the strong electrostatic attraction between the negatively charged SRHA and the positively charged SAM-NH$_3^+$ surface. Following rinsing with SRHA-free solutions and hence removal of any non-adsorbed SRHA from the flow through system, virus-containing solutions were delivered (t= 0 min). The same experimental procedure was used for the other DOMs. The adsorption of the viruses to the DOM adlayers was highly reproducible, as illustrated in **Figure S16b** in the form of overlapping adsorption profiles of Qβ on SRFA adlayers. The results of representative adsorption experiments at pH 5 to 8 and

at constant $I$ = 10 mM for MS2 and Qβ are shown in **Figure S16c** and for fr and GA in **Figure S16d**. The adsorption profiles show that MS2 and fr exhibited very limited to no adsorption at all test pH values, while GA, and Qβ exhibited more pronounced, pH dependent adsorption.
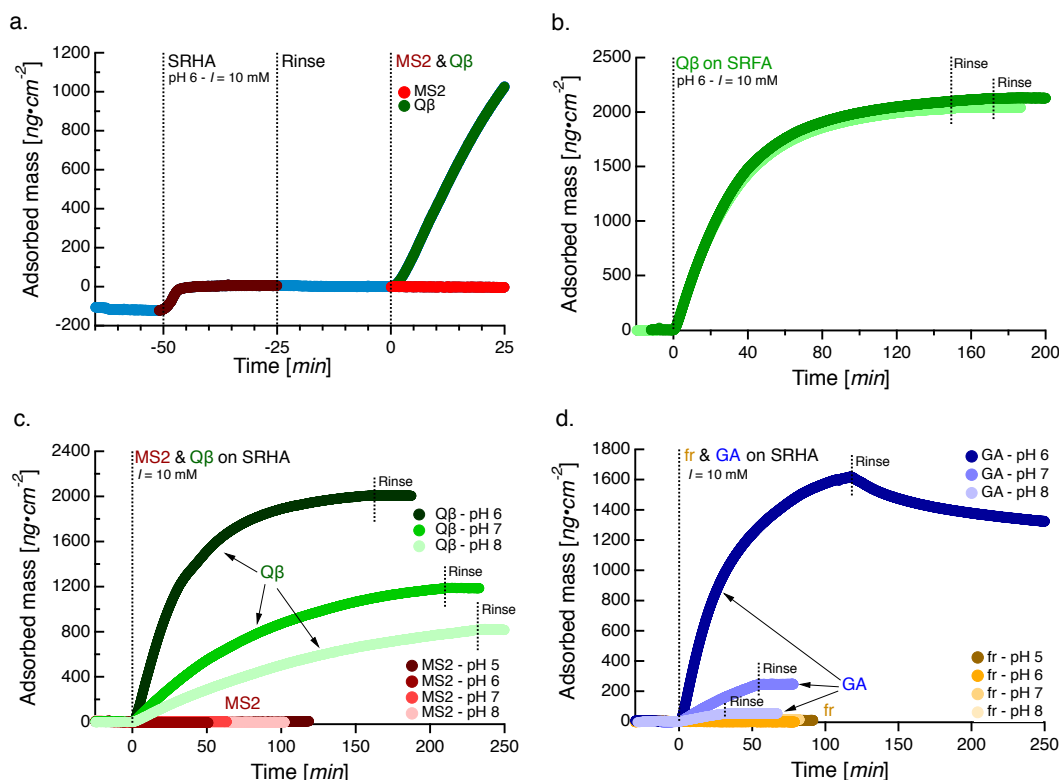


**Figure S16.** Adsorption profiles of MS2, fr, GA, and Qβ to dissolved organic matter (DOM) adlayers. (a) Adsorption profiles Suwannee River humic acid (SRHA) onto positively charged amine-terminated self-assembled monolayers (SAM-NH$_3^+$) and, after rinsing the system with SRHA-free solutions, of MS2 and Qβ to the formed SRHA adlayers, all at pH 6 and an ionic strength of $I$ = 10 mM (adjusted with NaCl). Panel (a) was replotted from **Figure 3b** in the manuscript. (b) Duplicate adsorption profiles of Qβ to Suwannee River fulvic acid (SRFA) adlayers at pH 6 and $I$ = 10 mM (adjusted with NaCl). (b) Representative adsorption profiles of MS2 and Qβ to SRHA adlayers at pH 5, 6, 7, and 8 and $I$ = 10 mM (adjusted by NaCl). (d) Representative adsorption profiles of fr and GA to SRHA adlayers at pH 5, 6, 7, and 8. All experiments were carried out at constant $I$ = 10 mM (adjusted with NaCl).

**Figure S17** shows representative adsorption profiles of MS2 (panel a) and Qβ (panel b) to SRHA, collected at pH 8 and $I$ of 10 and 100 mM (adjusted with NaCl as a background electrolyte).
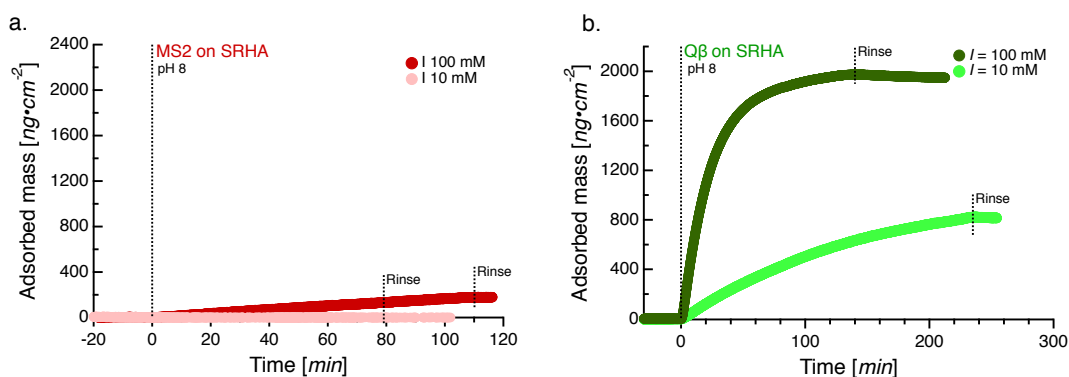
**Figure S17** Adsorption profiles of (a) MS2, and (b) Qβ onto Suwannee River humic acid (SRHA) surfaces, at pH 8 and $I$ = 10–100 mM with NaCl as a background electrolyte.

**Figure S18** shows the effect of solution $I$ on the $\alpha$ values of MS2 and MS2-VLP to SRHA and of MS2 to SRFA and ESHA adlayers, all at pH 6. For all tested DOMs, the initial adsorption kinetics of MS2 increased with increasing $I$ to $\alpha$ values of ≈ 0.1 at the highest tested $I$ of 500 mM. The differences in $\alpha$ values between MS2 and MS2-VLP were small (i.e., the maximum difference, at $I$ = 500 mM, was $\Delta\alpha$≈ 0.07, suggesting that there was only a small (if any) contribution from the ssRNA core in MS2 to the MS2-surface electrostatic interactions). If the negatively charged ssRNA core had significantly contributed to electrostatics, then significantly faster initial adsorption rates (and hence higher $\alpha$ values) would have been expected for the MS2-VLP (which would have carried a lower negative surface charge due to the loss of the ssRNA) than MS2 (which would have carried a higher negative surface charge due to the ssRNA core) to the like charged DOM adlayer surfaces. We note that MS2 adsorption to ESHA at $I$ = 500 mM could not be studied due to coagulation of ESHA under these high ionic strength conditions.
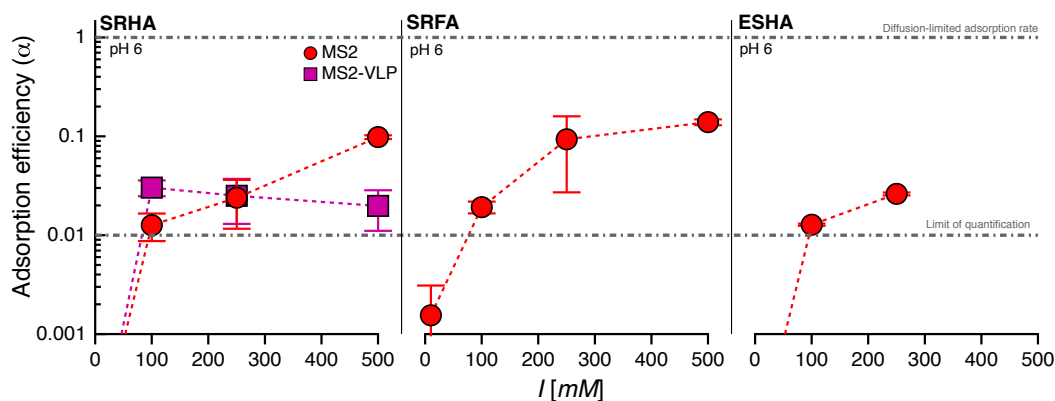
**Figure S18.** Adsorption efficiencies values, α, of MS2 and MS2-VLP to Suwannee River humic acid (SRHA), Suwannee River fulvic acid (SRFA) and Elliot Soil humic acid (ESHA) adlayers at pH 6 and increasing ionic strengths from $I$ of 10 to 500 mM (adjusted with NaCl). MS2 adsorption to ESHA adlayers at $I$ = 500 mM could not be studied as ESHA formed aggregates on the sensor surfaces under these high-$I$ conditions.

**Figure S19** shows the results of quadruplicate adsorption experiments of Qβ to SRHA adlayers at pH 6 ($I$ = 10 mM). Following attainment of the surface jamming limits (i.e., plateauing adsorption) and buffer rinsing at pH 6, the pH of the rinsing buffers was varied between the four parallel flow cells. Clearly, increasing the pH of the rinsing buffer increased the fraction of adsorbed Qβ that desorbed during the rinsing. This finding suggests that increasing solution pH caused significant increases in electrostatic repulsions between Qβ and the SRHA on some of the SRHA adsorption sites, resulting in desorption of Qβ. We note the final pH in all flow cells was brought back to pH 6 to compensate for pH buffer effects on the mass readings.
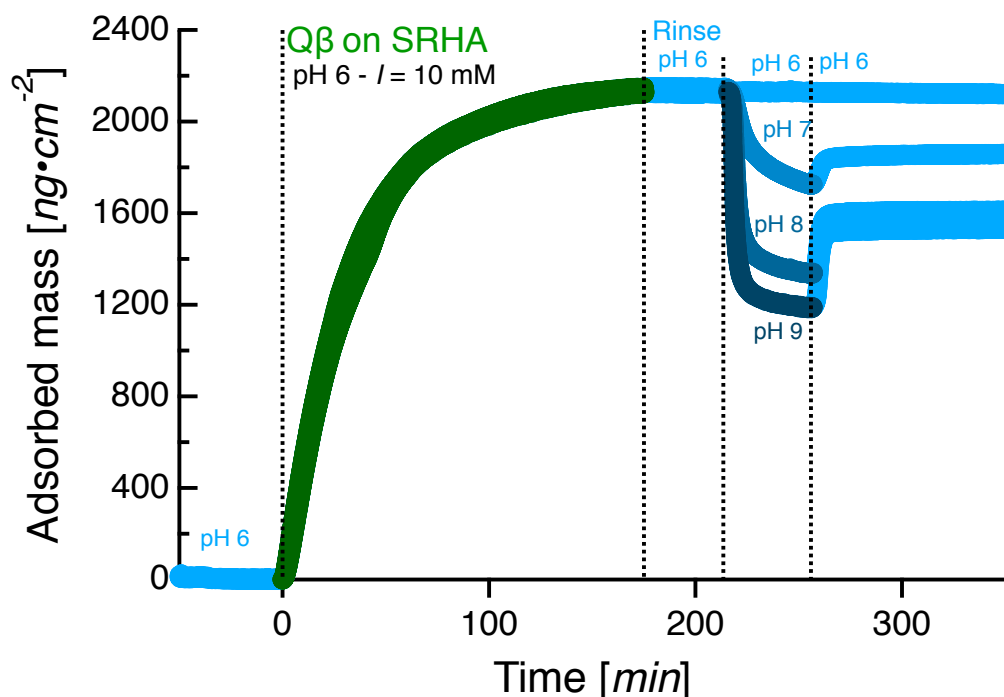
**Figure S19**. Changes in the adsorbed mass of Qβ on Suwannee River humic acid (SRHA) adlayers upon adsorption at pH 6 and upon rinsing with Qβ-free solutions of pH 6 in all cells and, subsequently, with pH 6, 7, 8, and 9 in the four parallel flow cells. A constant ionic strength of $I = 10$ mM (adjusted by NaCl) was maintained during the experiment.

# References

(1)    Golmohammadi, R.; Valegard, K.; Fridborg, K.; Liljas, L. The refined structure of bacteriophage MS2 at 2.8 Å resolution. *J. Mol. Biol.* **1993**, *234* (3), 620–639.

(2)    Liljas, L.; Fridborg, K.; Valegard, K.; Bundule, M.; Pumpens, P. Crystal structure of bacteriophage fr capsids at 3.5 Å resolution. *J. Mol. Biol.* **1994**, *244* (3), 279–290.

(3)    Tars, K.; Bundule, M.; Fridborg, K.; Liljas, L. The crystal structure of bacteriophage GA and a comparison of bacteriophages belonging to the major groups of *Escherichia coli leviviruses*. *J. Mol. Biol.* **1997**, *271* (5), 759–773.

(4)    Golmohammadi, R.; Fridborg, K.; Bundule, M.; Valegard, K.; Liljas, L. The crystal structure of bacteriophage Qβ at 3.5 angstrom resolution. *Structure* **1996**, *4* (5), 543–554.

(5)    Schrödinger, LLC. The PyMOL Molecular Graphics System, Version~1.3r1. August 2010.

(6)    Rumnieks, J.; Tars, K. Crystal Structure of the Bacteriophage Qβ Coat Protein in Complex with the RNA Operator of the Replicase Gene. *J. Mol. Biol.* **2014**, *426* (5), 1039–1049.

(7)    Carrillo-Tripp, M.; Shepherd, C. M.; Borelli, I. A.; Venkataraman, S.; Lander, G.; Natarajan, P.; Johnson, J. E.; Brooks, C. L.; Reddy, V. S. VIPERdb2: an enhanced and web API enabled relational database for structural virology. *Nucleic Acids Res.* **2009**, *37* (Database), D436–D442.

(8)    Pettersen, E. F.; Goddard, T. D.; Huang, C. C.; Couch, G. S.; Greenblatt, D.

M.; Meng, E. C.; Ferrin, T. E. UCSF Chimera–A visualization system for exploratory research and analysis. *J. Comput. Chem.* **2004**, *25* (13), 1605–1612.

(9)     Fraczkiewicz, R.; Braun, W. Exact and efficient analytical calculation of the accessible surface areas and their gradients for macromolecules. *J. Comput. Chem.* **1998**, *19* (3), 319–333.

(10)    Penrod, S. L.; Olson, T. M.; Grant, S. B. Deposition kinetics of two viruses in packed beds of quartz granular media. *Langmuir* **1996**, *12* (23), 5576–5587.

(11)    Li, H.; Robertson, A. D.; Jensen, J. H. Very fast empirical prediction and rationalization of protein pKa values. *Proteins* **2005**, *61* (4), 704–721.

(12)    Dolinsky, T. J.; Nielsen, J. E.; McCammon, J. A.; Baker, N. A. PDB2PQR: an automated pipeline for the setup of Poisson-Boltzmann electrostatics calculations. *Nucleic Acids Res.* **2004**, *32* (Web Server), W665–W667.

(13)    Dolinsky, T. J.; Czodrowski, P.; Li, H.; Nielsen, J. E.; Jensen, J. H.; Klebe, G.; Baker, N. A. PDB2PQR: expanding and upgrading automated preparation of biomolecular structures for molecular simulations. *Nucleic Acids Res.* **2007**, *35* (Web Server), W522–W525.

(14)    Kuhlman, B.; Baker, D. Native protein sequences are close to optimal for their structures. *P. Natl. Acad. Sci. USA* **2000**, *97* (19), 10383–10388.

(15)    Rohl, C. A.; Strauss, C. E.; Misura, K. M.; Baker, D. Protein structure prediction using Rosetta. *Methods Enzymol.* **2004**, *383*, 66–93.

(16)    Jacak, R.; Leaver-Fay, A.; Kuhlman, B. Computational protein design with explicit consideration of surface hydrophobic patches. *Proteins* **2011**, *80* (3), 825–838.

(17)    Armanious, A.; Aeppli, M.; Sander, M. Dissolved organic matter adsorption to model surfaces: adlayer formation, properties and dynamics at the nanoscale. *Environ. Sci. Technol.* **2014**, *48* (16), 9420–9429.

(18)    Hooker, J. M.; Kovacs, E. W.; Francis, M. B. Interior surface modification of bacteriophage MS2. *J. Am. Chem. Soc.* **2004**, *126* (12), 3718–3719.

(19)    Wigginton, K. R.; Menin, L.; Sigstam, T.; Gannon, G.; Cascella, M.; Hamidane, H. B.; Tsybin, Y. O.; Waridel, P.; Kohn, T. UV radiation induces genome-mediated, site-specific cleavage in viral proteins. *ChemBioChem* **2012**, *13* (6), 837–845.

(20)    Kropinski, A. M.; Mazzocco, A.; Waddell, T. E.; Lingohr, E.; Johnson, R. P. Enumeration of bacteriophages by double agar overlay plaque assay. In *Bacteriophages*; Springer, 2009; Vol. 1, pp 69–76.

(21)    Bingen, P.; Wang, G.; Steinmetz, N. F.; Rodahl, M.; Richter, R. P. Solvation effects in the quartz crystal microbalance with dissipation monitoring response to biomolecular adsorption. A phenomenological approach. *Anal. Chem.* **2008**, *80* (23), 8880–8890.

(22)    Overby, L. R.; Barlow, G. H.; Doi, R. H.; Jacob, M.; Spiegelman, S. Comparison of two serologically distinct ribonucleic acid bacteriophages I. Properties of the viral particles. *J. Bacteriol.* **1966**, *91* (1), 442.

(23)    Kyte, J.; Doolittle, R. F. A simple method for displaying the hydropathic character of a protein. *J. Mol. Biol.* **1982**, *157* (1), 105–132.

(24)    Paranchych, W.; Krahn, P. M.; Bradley, R. D. Stages in Phage R17 Infection. *Virology* **1970**, *41* (3), 465–473.

(25)    Roberts, J. W.; Steitz, J. E. The reconstitution of infective bacteriophage R17.

*P. Natl. Acad. Sci. USA* **1967**, *58* (4), 1416–1421.

(26)   Johannsmann, D.; Reviakine, I.; Richter, R. P. Dissipation in films of adsorbed nanospheres studied by quartz crystal microbalance (QCM). *Anal. Chem.* **2009**, *81* (19), 8167–8176.

(27)   Yuan, B.; Pham, M.; Nguyen, T. H. Deposition kinetics of bacteriophage MS2 on a silica surface coated with natural organic matter in a radial stagnation point flow cell. *Environ. Sci. Technol.* **2008**, *42* (20), 7628–7633.

(28)   Pham, M.; Mintz, E. A.; Nguyen, T. H. Deposition kinetics of bacteriophage MS2 to natural organic matter: role of divalent cations. *J. Colloid. Interf. Sci.* **2009**, *338* (1), 1–9.

(29)   Dika, C.; Gantzer, C.; Perrin, A.; Duval, J. F. L. Impact of the virus purification protocol on aggregation and electrokinetics of MS2 phages and corresponding virus-like particles. *Phys. Chem. Chem. Phys.* **2013**, *15* (15), 5691–5700.

(30)   Gregory, J. Approximate expressions for retarded van der Waals interaction. *J. Colloid. Interf. Sci.* **1981**, *83* (1), 138–145.

(31)   Murray, J. P.; Parks, G. A. Poliovirus adsorption on oxide surfaces: Correspondence with the DLVO-Lifshitz theory of colloid stability. In *Particulates in water*, Kavanaugh, M. C., Leckie, J. D., Eds.; American Chemical Society, Washington D.C. 1980; pp 97.

(32)   Murray, J. P. Physical chemistry of virus adsorption and degradation on inorganic surfaces. *US Environmental Protection Agency, Cincinnati, Ohio* **1980**.

(33)   Hogg, R.; Healy, T. W.; Fuerstenau, D. W. Mutual coagulation of colloidal dispersions. *Trans. Faraday Soc.* **1966**, *62*, 1638.

(34)   Israelachvili, J. N. *Intermolecular and surface forces*, Third Edition. Academic Pr, 2010.

(35)   Schweiss, R.; Welzel, P. B.; Werner, C.; Knoll, W. Dissociation of surface functional groups and preferential adsorption of ions on self-assembled monolayers assessed by streaming potential and streaming current measurements. *Langmuir* **2001**, *17* (14), 4304–4311.

(36)   Giesbers, M.; Kleijn, J. M.; Cohen Stuart, M. A. The electrical double layer on gold probed by electrokinetic and surface force measurements. *J. Colloid. Interf. Sci.* **2002**, *248* (1), 88–95.